AIP | The Journal of Chemical Physics

Photoelectron velocity-map imaging spectroscopic and theoretical study on the reactivity of the gold atom toward CH3SH, CH3OH, and H2O

Zhengbo Qin, Ran Cong, Xia Wu, Zhiling Liu, Hua Xie, Zichao Tang, Ling Jiang, and Hongjun Fan

Citation: The Journal of Chemical Physics **139**, 034315 (2013); doi: 10.1063/1.4813631
View online: http://dx.doi.org/10.1063/1.4813631
View Table of Contents: http://scitation.aip.org/content/aip/journal/jcp/139/3?ver=pdfcov
Published by the AIP Publishing

Photoelectron velocity-map imaging spectroscopic and theoretical study on the reactivity of the gold atom toward CH_3SH, CH_3OH, and H_2O

Zhengbo Qin, Ran Cong, Xia Wu, Zhiling Liu, Hua Xie, Zichao Tang,[a] Ling Jiang,[a] and Hongjun Fan[a]
State Key Laboratory of Molecular Reaction Dynamics, Dalian Institute of Chemical Physics, Chinese Academy of Sciences, Dalian 116023, China

(Received 26 April 2013; accepted 27 June 2013; published online 18 July 2013)

Photoelectron velocity-map imaging spectroscopy has been used to study the reaction of the anionic gold atom with the HR (R = SCH_3, OCH_3, OH) molecules. The solvated $[Au\cdots HR]^-$ and inserted $[HAuR]^-$ products have been experimentally observed for R = SCH_3, whereas only solvated $[Au\cdots HR]^-$ products were found for R = OCH_3 and OH. This significant difference in the photoelectron spectra suggests the different reactivity of the Au^- toward the CH_3SH, CH_3OH, and H_2O molecules. Second order Møller–Plesset perturbation theory and coupled-cluster single double triple excitation calculations have been performed to aid the structural assignment of the spectra and to explore the reaction mechanism. Activation energies for the isomerizations of the solvated structures to the inserted ones in the Au^-/Au + HR reactions (R = OCH_3 and OH) are predicted to be much higher than those for the Au^-/Au + CH_3SH reactions, supporting the experimental observation. Theoretical calculations provide the evidence that the intriguing $[HAuSCH_3]^-$ product may be formed by the attachment of the electron onto the neutral $HAuSCH_3$ species or the isomerization from the anionic $[Au\cdots HSCH_3]^-$ one. These findings should be helpful for understanding the feature that the thiols are able to form the staple motifs, whereas CH_3OH and H_2O are not. © *2013 AIP Publishing LLC*. [http://dx.doi.org/10.1063/1.4813631]

I. INTRODUCTION

The interaction of the thiols with gold surfaces and interfaces is of considerable interest, in that thiolate-protected gold nanoparticles and self-assembled monolayers are relevant for the design of new materials for molecular electronics and corrosion inhibition, the enhancement of the biocompatibility of materials, and the modifications of surface properties and heterogeneous catalysis.[1,2] One important milestone for the thiol chemistry is the structural characterization of two kinds of gold clusters, $Au_{102}(p\text{-MBA})_{44}$[3] and $Au_{25}(SR)_{18}$,[4–6] in which the staple RS–Au–SR and RS–Au–SR–Au–SR (R = organic group) motifs are identified. This stimulates the synthesis of a number of novel well-defined gold nanoparticles.[7–12] Scanning tunneling microscopic study on the adsorption of alkanethiols onto the Au (111) surface exhibits that the origin for driving self-assembly of Au–SR chain backbone is the gold adatom.[7,13–18]

Extensive efforts have been made to explore the formation mechanism for the staple bonding motifs. Experimentally, the loss of hydrogen has been observed upon the exposure of thiols to very large gold particles (∼4 nm, about Au_{2000} size).[19] Theoretical investigations have suggested a most likely pathway of S–H bond rupture of the CH_3SH molecule on the Au atom and Au_{20},[20] on Au_4[21] or gold surfaces,[22] namely, the co-adsorption of two or three CH_3SH molecules on the gold clusters induce the release of H_2 and the formation of the staple motif. Recent photoelectron spectroscopic and theoretical investigation reveals a covalent characteristic of the Au–S bond.[23] Compared to the feature of dissociative adsorption of the CH_3SH molecule on the gold nanoparticles and surfaces, the CH_3OH and H_2O molecules prefer the molecular adsorption on the clean surfaces.

Gas-phase study on the interaction of group 11 metal atoms with solvent molecules (i.e., CH_3SH, CH_3OH, H_2O) provides a simple model for understanding the nature of the solvation and the reactivity in the bulk phase. Recent experiments of infrared photodissociation spectroscopy gave access to vibrational frequencies and detailed structural information of $[M\cdot H_2O]^-\cdot Ar_n$ (M = Cu, Ag, Au; n = 1, 2).[24] Anion photodetachment-photoelectron imaging spectra of $[Cu\cdot(H_2O)_{1,2}]^-$ were reported by Lineberger and co-workers[25] using high resolution photoelectron imaging system.[26,27] Chi *et al.*[28,29] have obtained electron affinities, vibrational frequencies, structural information of $[Ag\cdot(H_2O)_{1,2}]^-$ and $[Ag\cdot(CH_3OH)_{1,2}]^-$ using photoelectron imaging system. Photoelectron spectra (PES) of $[Au\cdot(H_2O)_{1,2}]^-$ have been measured by Zheng *et al.*[30] Lineberger and co-workers[31–34] investigated the structural dynamics of the $[Cu\cdot(H_2O)]^-$, $[Cu\cdot(H_2O)_2]^-$, and $[Cu\cdot(CD_3OD)]^-$ complexes using femtosecond photodetachment-photoionization technique as well as high-level *ab initio* and wave-packet dynamics simulations. Tachikawa[35] recently reported an *ab initio* molecular

[a]Authors to whom correspondence should be addressed. Electronic addresses: zctang@dicp.ac.cn, ljiang@dicp.ac.cn, and fanhj@dicp.ac.cn. Tel.: +86-411-84379365. Fax: +86-411-84675584.

dynamics (AIMD) study on the electron detachment dynamics of $[Cu \cdot (H_2O)_n]^-$ ($n = 1$–3) and found that the structural change of $[Cu \cdot H_2O]^-$ involves three reaction channels. In these anionic $[M \cdots HR]^-$ (M = Au, Ag, Cu; R = OCH_3, OH) complexes, the charge is mainly localized on the anionic metal atoms. These investigations have been mainly focused on the determination of the geometrical structures and thermochemical information. However, much less work has been done on the understanding of the activation mechanism of O–H bond of CH_3OH and H_2O by the metal atoms. So far, the understanding of such difference in the reactivity of the gold atom toward the CH_3SH, CH_3OH, and H_2O molecules at the molecular level remains open.

In this work, we report a study of the reaction of the anionic gold atom with the HR (R = SCH_3, OCH_3, OH) molecules using a combined approach of photoelectron velocity-map imaging spectroscopy and quantum chemical calculations. The solvated $[Au \cdots HR]^-$ and inserted $[HAuR]^-$ products have been experimentally observed for R = SCH_3, whereas only solvated $[Au \cdots HR]^-$ products have been found for R = OCH_3 and OH. The second order Møller–Plesset perturbation (MP2) theory and coupled-cluster single double triple (CCSD (T)) calculations have been performed to elucidate the reaction mechanism of the anionic gold atom with the HR (R = SCH_3, OCH_3, OH) molecules.

II. EXPERIMENTAL AND COMPUTATIONAL METHODS

The experiments were performed using a laser ablation source and photoelectron velocity-map imaging system. The instrument has been described elsewhere.[36] Briefly, the second harmonic of Nd:YAG laser (532 nm, 10 Hz) was focused on the rotating gold target (99.9%) in the presence of a supersonic beam of helium (99.999%) carrier gas with 5% methanethiol (or bubbled water and methanol). The formed anions of interest were steered to a McLaren-Wiley time-of-flight, mass selected, and interacted with a laser beam of 355 nm or 266 nm from a Nd:YAG laser for the photodetachment. It was not necessary to subtract the background in the present experiments, because the background electrons were negligible. The resulting photoelectrons were extracted by a velocity map imaging photoelectron spectrometer and recorded by a charge-coupled device camera. Each image was accumulated with 10 000–50 000 laser shots at 10 Hz repetition rate. The final raw image stood for the projection of the photoelectron density in the 3D laboratory frame onto the 2D imaging detector. The original 3D distribution was reconstructed using the Basis Set Expansion (BASEX) inverse Abel transform method, and the photoelectron spectrum was acquired by integrating the central slice of the 3D distribution.[37] The photoelectron kinetic energy spectra were calibrated by the known spectrum of Au^-. The PES were plotted against electron binding energy eBE = hν − eKE, where hν is the photon energy. The typical energy resolution was about 30 meV full width at half maximum (FWHM) at electron kinetic energy (eKE) of 1 eV.

All theoretical calculations were carried out using the GAUSSIAN 09 package.[38] The basis set of aug-cc-pVTZ-pp[39–41] with the small core pseudopotentials was used for the gold atom, and aug-cc-pVTZ[42] for other atoms. The structures for the anionic and neutral complexes were optimized at the MP2 level.[43] Transition state (TS) geometries connecting the stable structures were searched at the same level and checked by calculating the intrinsic reaction coordinates (IRCs). Vibration analysis was employed to check it out whether the optimized structures were the true local minima or not. All the energies of the MP2 optimized structures were reevaluated at the coupled cluster CCSD (T)[44,45] level. The excitation energies were obtained by equation-of-motion coupled cluster calculations with singles and doubles (EOM-CCSD)[46] calculations. The adiabatic detachment energies (ADE) was defined as the energy of the origin transition between the ground state of the anion and the ground state of the neutral, which also represents the electron affinity of neutral species. The vertical detachment energy (VDE) was defined as the energy difference between the ground state of the anion and the ground state of the neutral at the anion geometry.

III. RESULTS AND DISCUSSION

A. Experimental results

Fig. 1 shows the 266 nm photoelectron velocity-map images and corresponding PES of the species from the Au^- + HR reactions (R = OH, OCH_3, SCH_3) and the comparison

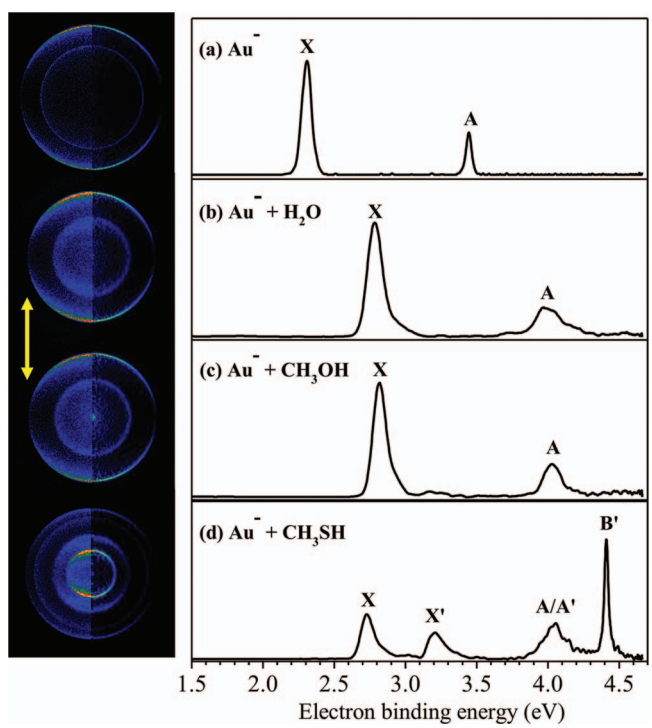

FIG. 1. Photoelectron velocity images (left columns) and photoelectron spectra (right columns) of (a) Au^-, (b) $Au^- + H_2O$, (c) $Au^- + CH_3OH$, (d) $Au^- + CH_3SH$ at 266 nm (4.661 eV), where X stands for the ground state of solvated $[Au \cdots HR]^-$, X′ for the ground state of inserted $[HAuR]^-$, A for the excited state of solvated $[Au \cdots HR]^-$, and A′, B′ for the first and second excited states of inserted $[HAuR]^-$. Each photoelectron velocity image consists of raw image (left part) and the reconstructed image (right part) after inverse Abel transformation. The double arrow indicates the directions of the laser polarization.

with the bare Au^- anion. The bands in the photoelectron spectrum represent the electron binding energies of photodetachment transitions from the ground state of the anionic cluster to the ground or excited states of corresponding neutral cluster. For the Au^- anion (Fig. 1(a)), two sharp bands (X and A) are observed, which correspond to the ground ($^2S_{1/2}$) and excited ($^2D_{5/2}$) states, respectively. Analogously, two bands (X and A) present in the Au^-+ HR reactions (R = OH, OCH_3, SCH_3) (Figs. 1(b)–1(d)), blue shifting by about 0.5 eV relative to the Au^- anion. Thus, the X and A bands in each reaction should be due to the ground and excited states of the solvated $[Au\cdots HR]^-$ products, respectively. Interestingly, two extra bands (X′ and B′) are observed in the $Au^- + CH_3SH$ reaction, but not in the $Au^- + H_2O$ and $Au^- + CH_3OH$ reactions, exhibiting the significant difference in the PES spectra. The observation of the X′ and B′ bands suggests the coexistence of different isomers in the $Au^- + CH_3SH$ reaction, implying the different reactivity of the Au^- anion toward the CH_3SH, CH_3OH, and H_2O molecules.

The 355 nm photoelectron velocity-map images and corresponding photoelectron spectra of the products from the $Au^- + HR$ reactions (R = OH, OCH_3, SCH_3) are shown in Fig. 2, indicating the details of the resolved vibrational structures. The Franck–Condon simulations were carried out using the PESCAL program[47] to extract the values for the ADEs and vibrational frequencies, as well as the vibrational temperature of the anions. The geometries were optimized and vibrational frequencies of the anionic and neutral states were calculated at MP2 level. The potentials of neutral and anionic species were modeled as Morse oscillators. The FWHM was set at 35 meV. The simulated vibrational temperature of the anion was obtained at 255 K. The simulation provides the relative intensities of mainly individual vibronic transitions,

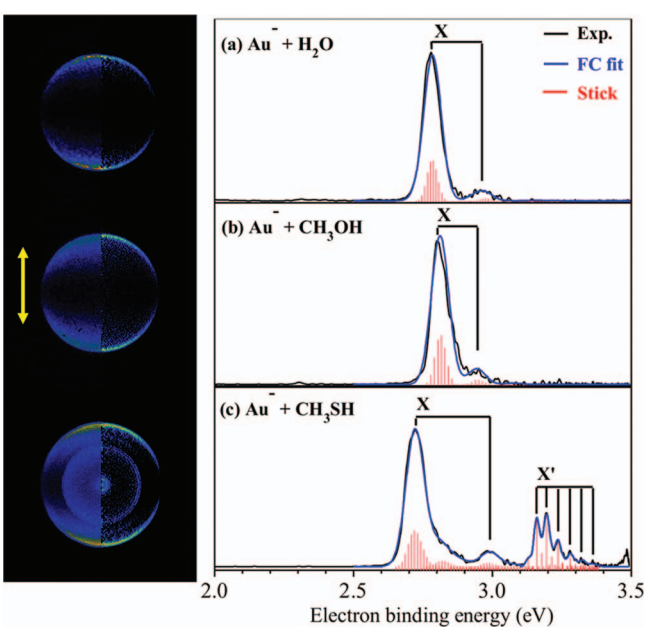

FIG. 2. Photoelectron velocity images (left columns) and photoelectron spectra (right columns) of (a) $Au^- + H_2O$, (b) $Au^- + CH_3OH$, and (c) $Au^- + CH_3SH$ at 355 nm (3.496 eV). Black curve stands for the experimental data, blue curves for Franck–Condon (FC) simulated results, and red sticks for simulated vibronic transitions.

TABLE I. Calculated and experimental adiabatic detachment energies (ADEs) and vertical detachment energies (VDEs) (eV) for the $[Au\cdots HR]^-$ and $[HAuR]^-$ species (R = SCH_3, OCH_3, OH).

	ADE		VDE		VDE (excited state)	
Species	Exp[a]	Cal	Exp[a]	Cal	Exp[a]	Cal
$[Au\cdots HSCH_3]^-$	···	2.596	2.729(33)	2.808	4.055(10)	4.229
$[HAuSCH_3]^-$	3.158(26)	3.145	3.207(25)	3.148	4.055(10)	4.120
					4.419(4)	4.641[b]
$[Au\cdots HOCH_3]^-$	···	2.748	2.815(32)	2.803	4.033(11)	4.406
$[HAuOCH_3]^-$	···	3.406	···	3.453	···	4.025
					···	4.590[b]
$[Au\cdots HOH]^-$	···	2.731	2.782(32)	2.783	3.996(11)	4.282
$[HAuOH]^-$	···	3.510	···	3.820	···	4.200
					···	4.696[b]

[a]Numbers in the parentheses are experimental uncertainties in the last digit.
[b]The calculated value of the second excited state.

which are displayed as red sticks in Fig. 2. The ADEs of band X in these three $Au^- + HR$ reactions cannot be determined because of no vibrational resolution. The ADE of band X′ in the $Au^- + CH_3SH$ reaction is determined at 3.158 eV. The vibrational frequencies for the X band and X′ bands are determined at 2194 ± 97 and 323 ± 21 cm^{-1}, respectively (Table I).

B. Theoretical results

In order to assign the PES spectra, theoretical calculations were carried out at the MP2 and CCSD (T) levels. Comparison of the theoretical and experimental vibrational frequencies, VDEs and ADEs are summarized in Table I. Optimized structures are depicted in Fig. 3. Considering that both the X and X′ bands are simultaneously observed in the $Au^- + CH_3SH$ reaction, the discussion will start with this reaction.

The inserted $[HAuSCH_3]^-$ structure (isomer II) is calculated to be the most stable isomer (Fig. 3). The solvated $[Au\cdots HSCH_3]^-$ structure (isomer I) lies 1.117 eV higher in energy than the isomer II. The VDEs of the ground state and the excited state of the $[Au\cdots HSCH_3]^-$ structure are predicted to be 2.808 and 4.229 eV, respectively, which are consistent with the experimental values of the X and A bands (2.729 and 4.055 eV) (Table I). Note that the A′ band (4.120 eV) of the $[HAuSCH_3]^-$ species overlaps with the A band of the $[Au\cdots HSCH_3]^-$ species (Fig. 1). The theoretical ADE and VDEs for $[HAuSCH_3]^-$ agree with the experimental values. The calculated S–H and Au–S stretching frequencies (2331 and 321 cm^{-1}) in the $[Au\cdots HSCH_3]^-/[HAuSCH_3]^-$ isomer are in accord with the experimental values (2194 ± 97 and 323 ± 21 cm^{-1}), respectively. Therefore, the X and X′ bands are assigned to the solvated $[Au\cdots HSCH_3]^-$ and inserted $[HAuSCH_3]^-$ isomers, respectively.

For the $Au^- + CH_3OH$ and $Au^- + H_2O$ reactions, the solvated structures (isomers III and V) are predicted to be the lowest-lying isomers, which are slightly more stable than the inserted structures (isomers IV and VI) (Fig. 3). It can be found from Table I that the calculated VDEs of

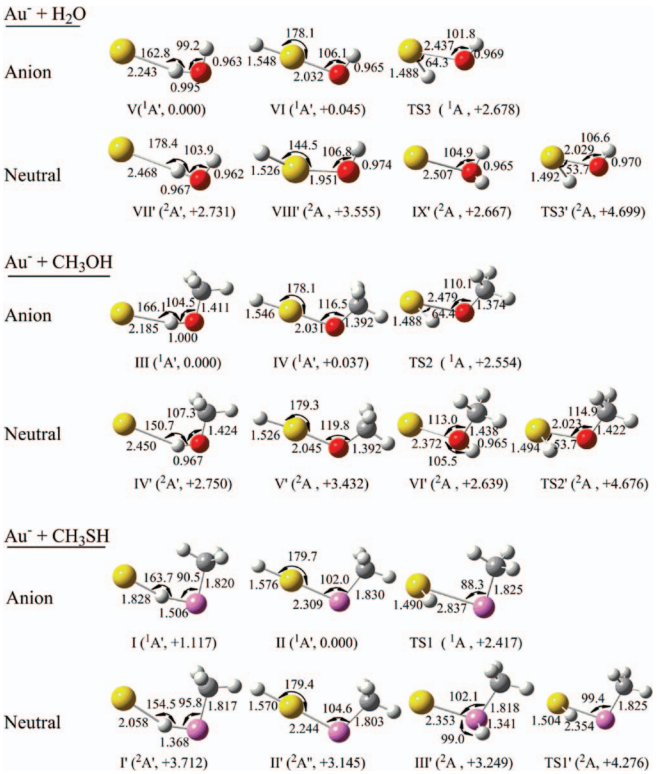

FIG. 3. Optimized structures of low-lying isomers for anionic and neutral species from the $Au^- + HR$ (R = OH, OCH_3, SCH_3) reactions. Relative energies (in eV) are given in the parentheses with respect to the ground state of the anion.

$[Au\cdots HOCH_3]^-$ and $[Au\cdots HOH]^-$ agree with the experimental values. The C–O–H bending vibration frequency in the $Au\cdots HOCH_3$ complex is calculated to be 1084 cm^{-1} and the H_2O bending vibration frequency in the $Au\cdots HOH$ complex to be 1616 cm^{-1}, respectively, which are in accord with the experimental values of 1080 ± 79 and 1557 ± 85 cm^{-1}.

C. Discussions

The reaction profiles for the $Au^-/Au + HR$ reactions (R = SCH_3, OCH_3, OH) are shown in Figs. 4–6. The calculated binding energy for the interaction of Au^- with CH_3SH is 0.488 eV (Fig. 4), which is 0.116 and 0.064 eV smaller than that with CH_3OH and H_2O (Figs. 5 and 6), respectively. This order is consistent with the experimental trend of blue shifting of band X ($[Au\cdots HSCH_3]^-$: 0.288 eV, $[Au\cdots HOH]^-$: 0.423 eV, $[Au\cdots HOCH_3]^-$: 0.440 eV) relative to the bare Au^- atom.

As indicated in Fig. 4, the formation of the solvated $[Au\cdots HSCH_3]^-$ species from the $Au^- + CH_3SH$ reaction is exothermic by 0.488 eV. The isomerization of the solvated $[Au\cdots HSCH_3]^-$ structure to the inserted $[HAuSCH_3]^-$ structure is exothermic by 1.116 eV with the activation energy of 1.301 eV. Then, the total reaction energy for the formation of the inserted $[HAuSCH_3]^-$ from the $Au^- + CH_3SH$ reaction is exothermic by 1.604 eV. In contrast, the formation of neutral $HAuSCH_3$ from the $Au + CH_3SH$ reaction is exothermic

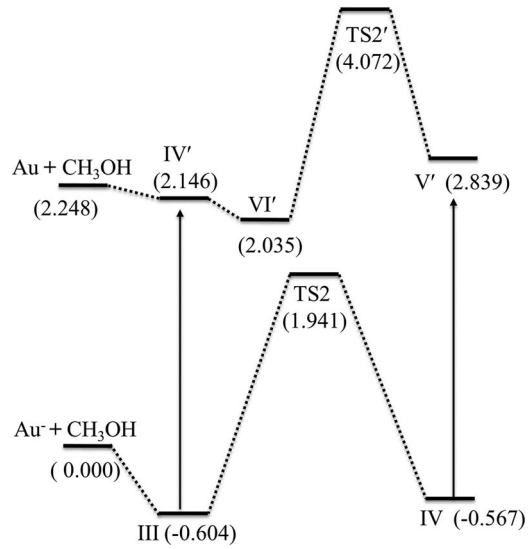

FIG. 5. The reaction profile for $Au^-/Au + CH_3OH$. Energies (in eV) are given in the parentheses.

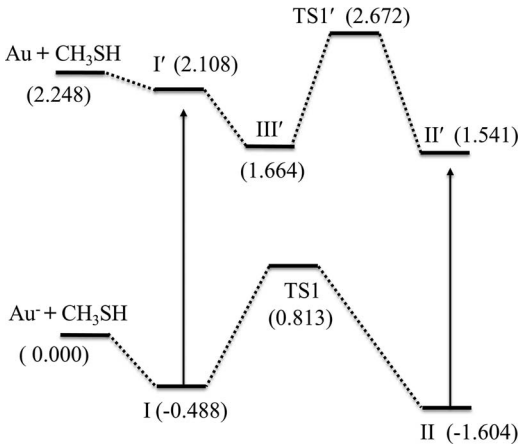

FIG. 4. The reaction profile for $Au^-/Au + CH_3SH$. Energies (in eV) are given in the parentheses.

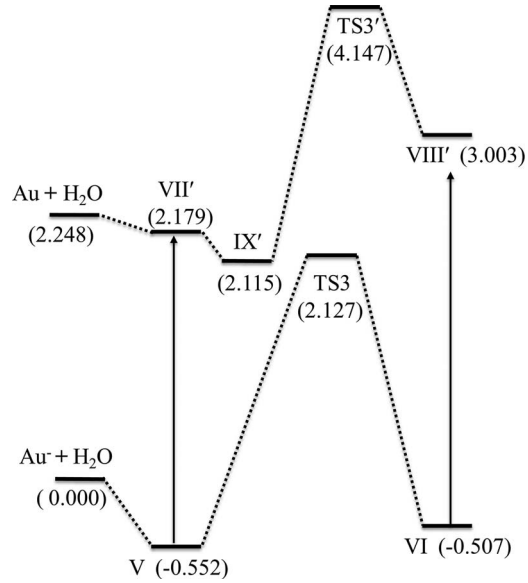

FIG. 6. The reaction profile for $Au^-/Au + H_2O$. Energies (in eV) are given in the parentheses.

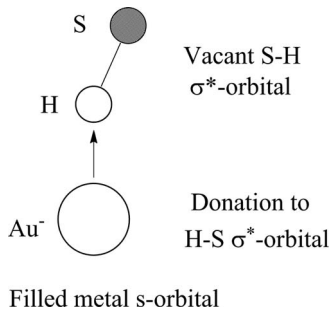

FIG. 7. Qualitative bonding description for the interactions of Au^- *s* orbital and H–S σ antibonding orbital.

by 0.707 eV. The activation barrier for the isomerization of the isomer III′ to the isomer II′ is 1.008 eV, which is slightly lower than that of the isomer I to the isomer II.

One reaction pathway for the formation of $[HAuSCH_3]^-$ is that the inserted neutral $HAuSCH_3$ is first generated from the reaction of neutral gold atom with CH_3SH in the source region and then the anionic $[HAuSCH_3]^-$ species is formed by attaching electron onto the neutral $HAuSCH_3$ one. Note that the ADE of the neutral insertion product $HAuSCH_3$ (3.145 eV) is higher than that of the neutral solvation product (2.596 eV). Considering that the isomer with a higher vertical electron affinity (VEA) could be readily observed,[48] the formation of the $[HAuSCH_3]^-$ species from the attachment of the electron onto the neutral $HAuSCH_3$ species is thus possible. Another pathway for the formation of the $[HAuSCH_3]^-$ species is that the $[Au\cdots HSCH_3]^-$ species is directly generated from the $Au^- + CH_3SH$ reaction and then isomerizes to the inserted structure. Since the activation energies for the isomerizations (∼1 eV) in the $Au^-/Au + CH_3SH$ reactions are readily overcome in the supersonic molecular beam, these two pathways should be responsible for the formation of $[HAuSCH_3]^-$.

In contrast to the reaction energies for the formation of the inserted $[HAuSCH_3]^-/HAuSCH_3$ products from the $Au^-/Au + CH_3SH$ reactions (−1.604/−0.707 eV), these for the $[HAuOCH_3]^-/HAuOCH_3$ and $[HAuOH]^-/HAuOH$ species are calculated to be −0.567/+0.591 and −0.507/+0.755 eV, respectively. The activation energy for the isomerization of the anionic solvated structure to the inserted one in the $Au^- + CH_3OH$ reaction is 2.545 eV (Fig. 5) and that in the $Au + CH_3OH$ reaction is 2.037 eV, which both are much higher than those in the $Au^-/Au + CH_3SH$ reactions (1.301 and 1.008 eV). Higher activation energies for the isomerizations have also been found in the $Au^-/Au + H_2O$ reactions (2.679 and 2.032 eV) (Fig. 6). Thus, both kinetic and thermodynamic data suggest that the formation of the inserted $[HAuOCH_3]^-$ and $[HAuOH]^-$ products is unfavorable in finite time (one experimental cycle: millisecond), consistent with their absence in the present experiments.

The interaction between the anionic Au^- atom and the HR molecules can be characterized as metal hydrogen bond where Au donate its 6*s* electrons to the S–H/O–H σ^* orbital of the ligand,[49] as shown in Fig. 7. Unlike the conventional hydrogen bond in which the electrostatics is the dominant contribution to the interaction energy, the polarization is the most important for metal hydrogen bond. Therefore, it is not surprising that the $Au^-\cdots CH_3SH$ interaction is stronger than the $Au^-\cdots CH_3OH$ and $Au^-\cdots H_2O$ interactions, because S–H bond is easier to be polarized than O–H bond. Natural population analysis (NPA)[50] also supports the larger charge transfer in the $Au^-\cdots CH_3SH$ system (0.28 e) than that in $Au^-\cdots H_2O$ and $Au^-\cdots CH_3OH$ (less than 0.1 e). As the results, in $Au^-\cdots CH_3SH$, the S–H bond length is quite long (1.506 Å, compared to 1.336 Å free CH_3SH) and Au–H bond length is pretty short (1.828 Å, compared to >2 Å in $Au^-\cdots H_2O$ and $Au^-\cdots CH_3OH$). The detailed geometric parameters can be found in Fig. S2 of the supplementary material.[51] The calculated Mayer bond order also shows that the $Au^-\cdots CH_3SH$ interaction is stronger than the $Au^-\cdots CH_3OH$ and $Au^-\cdots H_2O$ interactions (Table SI of the supplementary material).[51] The $Au\cdots CH_3SH$ interaction is also stronger than the $Au\cdots CH_3OH$ and $Au\cdots H_2O$ interactions, which causes shortening of the Au–H bond length (2.058 Å, compared to >2.4 Å in $Au\cdots H_2O$ and $Au\cdots CH_3OH$). However, the charge transfer in the neutral system is much less than that in the anionic one. So, the S–H bond length is nearly identical to that of free CH_3SH

TABLE II. Calculated NPA charge for solvated and inserted complexes in the $Au^- + HR$ (R = OH, OCH_3, SCH_3) reactions at the CCSD (T) level.

	Charge population			
Complex	NPA (Au)	NPA (S)	NPA (O)	NPA (H)[a]
$[Au\cdots HSCH_3]^{-1/0}$	− 0.719 (−0.034)[b]	− 0.264 (0.004)		0.102 (0.032)
$[HAuSCH_3]^{-1/0}$	0.085 (0.118)	− 0.486 (−0.298)		− 0.438 (−0.357)
$[Au\cdots HOCH_3]^{-1/0}$	− 0.912 (0.012)		− 0.846 (−0.760)	0.486 (0.447)
$[HAuOCH_3]^{-1/0}$	0.226 (0.227)		− 0.985 (−0.255)	− 0.418 (−0.310)
$[Au\cdots HOH]^{-1/0}$	− 0.939 (0.012)		− 1.001 (−0.924)	0.491 (0.452)
$[HAuOH]^{-1/0}$	0.228 (0.712)		− 1.217 (−0.982)	− 0.423 (−0.188)
$[Au\cdots SHCH_3]$	(− 0.158)	(0.066)		(0.117)
$[Au\cdots OHCH_3]$	(− 0.028)		(− 0.784)	(0.476)
$[Au\cdots OH_2]$	(− 0.018)		(− 0.940)	(0.479)

[a]The NPA (H) denotes the charge of hydrogen atom interacting with Au.
[b]Numbers in the parentheses denote the data for neutral species.

molecule. Additionally, the S–H bond energy is quite small compared to the bond energy of O–H bond. Two factors above-mentioned together result in the activation of S–H bond with much less activation energy, consistent with experimental observation of the inserted $[HAuSCH_3]$ isomer (Table II).

Previous theoretical investigations predicted that the RS–Au–SR staple motif were formed from the co-adsorption of two CH_3SH molecules on metal atom.[20] Based on the above analysis of the reaction energies and activation barriers for the $Au^-/Au + CH_3SH$ reactions, a plausible stepwise pathway for the formation of the staple motifs ($Au^-/Au + HSCH_3 \rightarrow [Au\cdots HSCH_3]^-/Au\cdots HSCH_3 \rightarrow [HAuSCH_3]^-/HAuSCH_3$, $[HAuSCH_3]^-/HAuSCH_3 + HSCH_3 \rightarrow [CH_3SAuSCH_3]^-/CH_3SAuSCH_3 + H_2$) is proposed. In fact, the $[HAuSCH_3]^-$ intermediate and the $[CH_3SAuSCH_3]^-$ products simultaneously present in the $Au^- + CH_3SH$ reaction (Fig. S1 of the supplementary material),[51] supporting this formation mechanism.

IV. CONCLUSIONS

In summary, the reaction of the anionic gold atom with the HR (R = SCH_3, OCH_3, OH) molecules has been studied using photoelectron velocity-map imaging spectroscopy and quantum chemical calculation. Overall agreement between the experimental and calculated photoelectron spectra as well as the vertical detachment energies allows for structural assignment to be established. The solvated $[Au\cdots HR]^-$ and inserted $[HAuR]^-$ products have been experimentally observed for R = SCH_3, whereas only solvated $[Au\cdots HR]^-$ products have been found for R = OCH_3 and OH, implying the significant difference in the reactivity of the Au^- anion toward the CH_3SH, CH_3OH, and H_2O molecules. MP2 and CCSD (T) calculations predict that activation energies for the isomerizations of the solvated structures to the inserted ones in the $Au^-/Au+$ HR reactions (R = OCH_3 and OH) are much higher than those in the $Au^-/Au + CH_3SH$ reactions, supporting the experimental observation. The metal hydrogen bond interaction in the Au^-LHR systems reveals that the activation of the CH_3SH molecule is dependent on the polarization and weak bond energy of the S–H bond. The intriguing $[HAuSCH_3]^-$ product may be formed by the attachment of the electron onto the neutral $HAuSCH_3$ species or the isomerization from the anionic $[Au\cdots HSCH_3]^-$ species. These findings should be helpful for understanding the feature that the thiols are able to form the staple motifs, whereas CH_3OH and H_2O are not.

ACKNOWLEDGMENTS

This work is supported by the National Natural Science Foundation of China (NSFC) (Grant Nos. 21103186, 21073186, and 21273233), the Ministry of Science and Technology of China (Grant Nos. 2011CB201301 and 2011YQ09000505), and the Chinese Academy of Sciences.

[1] M. C. Daniel and D. Astruc, Chem. Rev. **104**, 293 (2004).
[2] J. C. Love, L. A. Estroff, J. K. Kriebel, R. G. Nuzzo, and G. M. Whitesides, Chem. Rev. **105**, 1103 (2005).
[3] P. D. Jadzinsky, G. Calero, C. J. Ackerson, D. A. Bushnell, and R. D. Kornberg, Science **318**, 430 (2007).
[4] J. Akola, M. Walter, R. L. Whetten, H. Häkkinen, and H. Grönbeck, J. Am. Chem. Soc. **130**, 3756 (2008).
[5] M. W. Heaven, A. Dass, P. S. White, K. M. Holt, and R. W. Murray, J. Am. Chem. Soc. **130**, 3754 (2008).
[6] M. Zhu, C. M. Aikens, F. J. Hollander, G. C. Schatz, and R. Jin, J. Am. Chem. Soc. **130**, 5883 (2008).
[7] D.-E. Jiang, M. L. Tiago, W. Luo, and S. Dai, J. Am. Chem. Soc. **130**, 2777 (2008).
[8] A. Dass, J. Am. Chem. Soc. **131**, 11666 (2009).
[9] M. Zhu, H. Qian, and R. Jin, J. Am. Chem. Soc. **131**, 7220 (2009).
[10] H. Qian, W. T. Eckenhoff, Y. Zhu, T. Pintauer, and R. Jin, J. Am. Chem. Soc. **132**, 8280 (2010).
[11] P. R. Nimmala and A. Dass, J. Am. Chem. Soc. **133**, 9175 (2011).
[12] H. Qian and R. Jin, Chem. Mater. **23**, 2209 (2011).
[13] P. Maksymovych, D. C. Sorescu, and J. T. Yates, Jr., Phys. Rev. Lett. **97**, 146103 (2006).
[14] H. Grönbeck and H. Häkkinen, J. Phys. Chem. B **111**, 3325 (2007).
[15] P. Maksymovych and J. T. Yates, J. Am. Chem. Soc. **130**, 7518 (2008).
[16] P. Carro, R. Salvarezza, D. Torres, and F. Illas, J. Phys. Chem. C **112**, 19121 (2008).
[17] O. Voznyy, J. J. Dubowski, J. T. Yates, and P. Maksymovych, J. Am. Chem. Soc. **131**, 12989 (2009).
[18] P. Maksymovych, O. Voznyy, D. B. Dougherty, D. C. Sorescu, and J. T. Yates, Jr., Prog. Surf. Sci. **85**, 206 (2010).
[19] J. E. Matthiesen, D. Jose, C. M. Sorensen, and K. J. Klabunde, J. Am. Chem. Soc. **134**, 9376 (2012).
[20] M. Askerka, D. Pichugina, N. Kuz'menko, and A. Shestakov, J. Phys. Chem. A **116**, 7686 (2012).
[21] V. Rojas-Cervellera, E. Giralt, and C. Rovira, Inorg. Chem. **51**, 11422 (2012).
[22] M. Jaccob, G. Rajaraman, and F. Totti, Theor. Chem. Acc. **131**, 1150 (2012).
[23] C.-G. Ning, X.-G. Xiong, Y.-L. Wang, J. Li, and L.-S. Wang, Phys. Chem. Chem. Phys. **14**, 9323 (2012).
[24] H. Schneider, A. D. Boese, and J. M. Weber, J. Chem. Phys. **123**, 084307 (2005).
[25] G. J. Rathbone, T. Sanford, D. Andrews, and W. C. Lineberger, Chem. Phys. Lett. **401**, 570 (2005).
[26] F. Misaizu, K. Tsukamato, M. Sanekata, and K. Fuke, Laser Chem. **15**, 195 (1995).
[27] F. Misaizu, K. Tsukamoto, M. Sanekata, and K. Fuke, Surf. Rev. Lett. **03**, 405 (1996).
[28] C. Chi, H. Xie, Y. Li, R. Cong, M. Zhou, and Z. Tang, J. Phys. Chem. A **115**, 5380 (2011).
[29] C.-X. Chi, H. Xie, R. Cong, Z.-C. Tang, and M.-F. Zhou, Chin. J. Chem. Phys. **24**, 557 (2011).
[30] W. Zheng, X. Li, S. Eustis, A. Grubisic, O. Thomas, H. de Clercq, and K. Bowen, Chem. Phys. Lett. **444**, 232 (2007).
[31] M. S. Taylor, F. Muntean, W. C. Lineberger, and A. B. McCoy, J. Chem. Phys. **121**, 5688 (2004).
[32] F. Muntean, M. S. Taylor, A. B. McCoy, and W. C. Lineberger, J. Chem. Phys. **121**, 5676 (2004).
[33] M. S. Taylor, J. Barbera, C.-P. Schulz, F. Muntean, A. B. McCoy, and W. C. Lineberger, J. Chem. Phys. **122**, 054310 (2005).
[34] J. Barbera, S. Horvath, V. Dribinski, A. B. McCoy, and W. C. Lineberger, J. Chem. Phys. **126**, 084307 (2007).
[35] H. Tachikawa, RSC Adv. **2**, 12346 (2012).
[36] W. Xia, Q. Zheng-Bo, X. Hua, W. Xiao-Hu, C. Ran, and T. Zi-Chao, Chin. J. Chem. Phys. **23**, 373 (2010).
[37] V. Dribinski, A. Ossadtchi, V. A. Mandelshtam, and H. Reisler, Rev. Sci. Instrum. **73**, 2634 (2002).
[38] M. J. Frisch, G. W. Trucks, and H. B. Schlegel *et al.*, GAUSSIAN 09, Revision A.02, Gaussian, Inc., Wallingford, CT, 2009.
[39] D. E. Woon and J. T. H. Dunning, J. Chem. Phys. **98**, 1358 (1993).
[40] R. A. Kendall, J. T. H. Dunning, and R. J. Harrison, J. Chem. Phys. **96**, 6796 (1992).
[41] K. A. Peterson and C. Puzzarini, Theor. Chem. Acc. **114**, 283 (2005).
[42] J. T. H. Dunning, J. Chem. Phys. **90**, 1007 (1989).
[43] C. Møller and M. S. Plesset, Phys. Rev. **46**, 618 (1934).
[44] G. D. Purvis III and R. J. Bartlett, J. Chem. Phys. **76**, 1910 (1982).
[45] G. E. Scuseria, C. L. Janssen, and H. F. Schaefer III, J. Chem. Phys. **89**, 7382 (1988).

[46]T. Korona and H.-J. Werner, J. Chem. Phys. **118**, 3006 (2003).
[47]K. M. Ervin, T. M. Ramond, G. E. Davico, R. L. Schwartz, S. M. Casey, and W. C. Lineberger, J. Phys. Chem. A **105**, 10822 (2001).
[48]L. Kronik, R. Fromherz, E. Ko, G. Gantefor, and J. R. Chelikowsky, Nature Mater. **1**, 49 (2002).
[49]L. Brammer, Dalton Trans. **2003**, 3145.
[50]A. E. Reed, L. A. Curtiss, and F. Weinhold, Chem. Rev. **88**, 899 (1988).
[51]See supplementary material at http://dx.doi.org/10.1063/1.4813631 for complete Ref. 38, mass spectra of the products from the $Au^- + CH_3SH$ reaction, and charge transfer and bond lengths in the solvated complexes.